ingegneria sismica
International Journal of Earthquake Engineering
Anno XLIII - Num. 3 - 2026

A Power Surge Suppression Method for Charge–Discharge Switching of Energy Storage Systems in Power Plants

Shiyu Zhang[1,*]

[1] College of Electrical and Electronic Engineering, Wenzhou University, Wenzhou 325035, Zhejiang, China

SUMMARY: *Utility-scale battery energy storage systems undergo frequent charge–discharge mode transitions, inducing severe power surges that threaten power converter reliability and grid interface stability. Existing solutions primarily address steady-state power smoothing or mode transitions in residential-scale inverters. Consequently, the rapid bidirectional power reversals inherent in utility-scale storage systems remain largely underexplored. This paper identifies a transient power surge mechanism in dual-active-bridge (DAB) based storage converters, revealing that phase-shift discontinuity during mode reversal is the root cause of instantaneous power spikes. A composite control strategy is proposed, integrating a transient phase-shift feedforward compensator with an adaptive virtual impedance regulator. Unlike conventional mode-switching methods that rely on control loop replacement, the proposed approach maintains a unified control architecture and dynamically reshapes the transient power trajectory via pre-positioned phase-shift adjustments and impedance regulation. A 500-kW energy storage converter hardware-in-the-loop platform is constructed.Experimental results demonstrate that the proposed method reduces the peak power surge by 74.6%, shortens the switching transient duration from 1.21 s to 0.28 s, and limits DC bus voltage deviation to within ±3.8%. Furthermore, the proposed method exhibits superior transient suppression performance compared with conventional PI-based mode switching and droop-only control under various states of charge (SOC) and power deficit conditions.*

KEYWORDS: *Power surge suppression; charge–discharge switching; dual active bridge; transient phase-shift compensation; energy storage converter*

1 Introduction

Battery energy storage systems integrated into power plants enable frequency regulation, renewable smoothing, and peak shaving services. However, unlike residential or commercial storage inverters that operate in steady state without frequent mode transitions, plant-level storage systems experience rapid bidirectional power fluctuations dispatched by grid operators. Consequently, safety and integrity risks induced by power surges during charge–discharge mode switching have not been sufficiently investigated[1].

The primary two classes of existing research focused on the suppression of power fluctuations in energy storage systems can be described as follows. The first class includes steady-state power smoothing approaches which utilize low-pass filters, wavelet packets, or model predictive control to assign high-frequency fluctuations to supercapacitors, batteries to low-frequency components. They deal with the uncertainty of renewable generation, however,

*zsyu040302@126.com
https://doi.org/10.65102/is20261137
Published: 10 June, 2026

they operate under the assumption of uninterrupted operation in a single operational regime. The second class primarily centers on the control of operational mode transitions, which has been particularly well studied in the area of residential storage inverters and uninterruptible power supplies. The most fundamental problem shown in Fig. 1, and the problem this paper addresses, is that the charging and discharging operational modes involve a rapid reversal of power flow, resulting in a transient power spike at the converter.

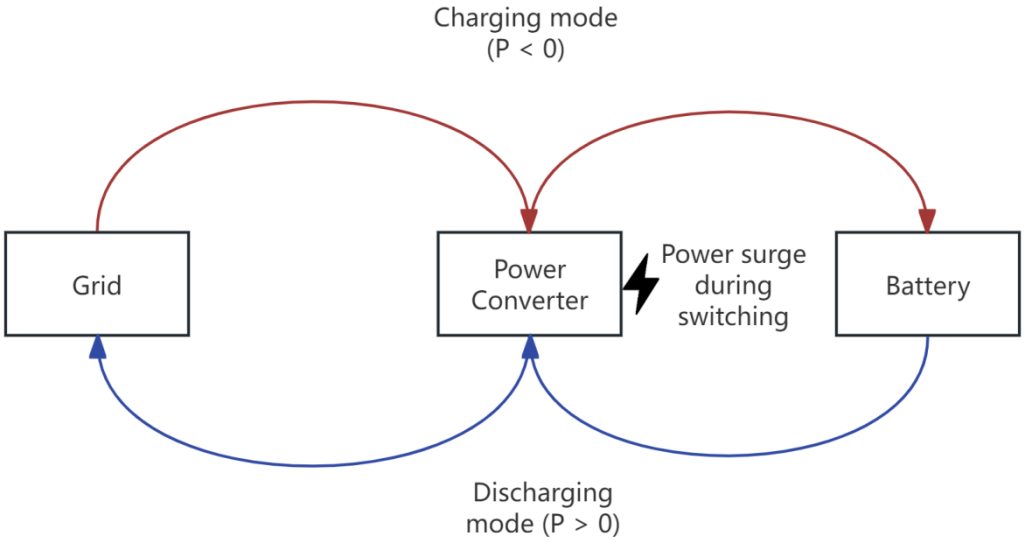

Figure 1: Schematic diagram of charge-discharge mode transition

A unified power control loop eliminating control loop switching was proposed for 5-kW residential inverters, achieving a transition time of approximately 1.18 s [2]. Flywheel energy storage systems have employed flux linkage angle compensation to suppress voltage/current spikes during mode switching, achieving an 11–30% oscillation reduction [3]. Voltage droop-based strategies for dual-active-bridge converters have demonstrated improved off-grid transient response, reducing power overshoot from 28.87% to 4.27% [4].

Despite these contributions, three major gaps still exist. First, studies on mode switching have only been conducted on low-power (<10 kW) residential systems, where switching is less frequent and the ability to tolerate surges is greater. No analysis has been conducted on the power surge mechanisms for bidirectional power reversals occurring rapidly in megawatt-class converters that have large DC-link capacitances, high switching frequency, and tighter grid code compliance. Second, traditional switching control approaches implement control loop switching (e.g., from charging PI control loop to discharging PI control loop) that are bound to cause signal discontinuities, leading to the emergence of power spikes. Finally, the role of the converter's internal phase-shift dynamics and the external droop support grid interaction at the moment of switching has not been investigated.

This paper addresses these gaps through the following contributions:

(1) A transients Power surge Model of a DAB-based Storage converter when in Bi-directional mode switching is created to derive an analytical expression that links phase-shift discontinuities to peak values of instantaneousenergy spikes.

(2) A transient phase-shift feedforward compensation framework is proposed, which pre-positions the phase-shift angle prior to mode switching and dynamically reshapes the post-switching trajectory without altering the unified control architecture.

(3) An adaptive virtual impedance regulator is synthesized with the feedforward compensator, enabling coordinated suppression of both power surge and DC bus voltage

deviation.

(4) Comprehensive hardware-in-the-loop (HIL) verification of the method on a 500-kW converter platform evaluates its effectiveness in various power deficits and SOCs compared to advanced standards.

2 Mechanism Analysis of Power Surge during Charge–Discharge Switching

2.1 System Configuration and DAB Operating Principles

The plant-level energy storage system examined here implements a dual-active-bridge topology as the bidirectional DC-DC interface between the battery bank and the DC bus. The DAB topology is chosen for its high power density, soft-switching, and bidirectional power flow features[5].

Under single-phase-shift modulation, the power transmission expression is well-established:

$$P=\frac{nU_{ba}U_{dc}\varphi(1-2|\varphi|)}{2f_sL} \quad \varphi\in[-0.25,0.25] \tag{1}$$

where φ denotes the phase-shift ratio between primary and secondary bridge voltages, positive φ indicates power flow from battery to DC bus (discharging), and negative φ corresponds to charging mode. Equation (1) exhibits odd symmetry: P(φ) = −P(−φ), with maximum power magnitude at |φ| = 0.25.

For small-signal dynamics around an operating point, the reduced-order model represents the DAB as a controlled current source. The secondary-side average current $\langle i_{b2}\rangle$ relates to phase shift by:

$$\langle i_{b2}\rangle=\frac{nU_{bat}\varphi(1-2|\varphi|)}{2f_sL} \tag{2}$$

2.2 Transient Surge Generation Mechanism

Traditional mode switching functions like this: in charging mode, φ = φ_c < 0; upon receiving a mode reversal command, the controller resets the phase-shift reference from φ_c to φ_d> 0 through a PI regulator with limited slew rate. However, because of the aforementioned digital control delay, anti-windup of the integrator, and the phase-shift initialization sequence, a momentary asynchrony happens—the phase-shift ratio does not continuously pass through zero but rather jumps or has a zero-crossing dead-zone.

Let φ(t) represent the instantaneous phase-shift trajectory during switching. The ideal trajectory φ*(t) should monotonically increase from $\varphi_c$to φ_d with bounded derivative. The actual trajectory, constrained by the modulator update mechanism and controller saturation, exhibits:

$$\varphi(t)=\begin{cases}\varphi_c, & t<t_0\\ \varphi_{\mathrm{hold}}, & t_0\le t<t_1\\ \varphi_d, & t\ge t_2\end{cases} \tag{3}$$

where [t0, t1] represents the phase-shift holding interval due to mode transition logic, and [t1,

t2] is the PI recovery interval. The instantaneous power at the switching instant becomes:

$$P_{surge}=\frac{nU_{bat}U_{dc}\varphi_{jump}(1-2|\varphi_{jump}|)}{2f_sL} \tag{4}$$

where φ_{jump} = φ(t1) − φ(t0−) is the effective phase-shift discontinuity. This discontinuity does not arise from some physical impossibility of a continuous phase shift, but rather from the control architecture where charging and discharging are treated as two separate operational modes with different regulator instances.

Additionally, during the holding interval, the battery current is suddenly cut off, which causes ringing of the inductor current. This phenomenon leads to the injection of extra transient energy into the DC-link capacitor. The DC bus voltage deviationΔU_{dc} is related to the energy surge ΔE by:

$$\Delta U_{dc}=\sqrt{\frac{2\Delta E}{C_{dc}}+U_{dc0}^2}-U_{dc0}\approx\frac{\Delta E}{C_{dc}U_{dc0}} \tag{5}$$

Table 1 quantifies the relationship between phase-shift discontinuity magnitude and resulting power surge based on (4), assuming a 500-kW DAB converter with parameters: U_{bat} = 800 V, U_{dc} = 750 V, f_s = 10 kHz, L = 50 μH, n = 1.

Table 1: Power Surge Magnitude versus Phase-Shift Discontinuity

φ_jump	P_{surge} (kW)	Per-unit Value	U_{dc} Drop (V)
0.05	225	0.45	18.3
0.10	400	0.80	32.6
0.15	525	1.05	42.8
0.20	600	1.20	48.9

Data indicate that even a phase-shift jump of 0.10 (40% of full-scale range) results in a 400-kW power surge—80% of rated power—within hundreds of microseconds. This surge effect arrives at the grid-side inverter, possibly activating overcurrent protection or causing AC-side frequency transients.

2.3 Limitations of Conventional Suppression Approaches

The previous suppression strategy adds a rate limiter to the phase-shift reference. However, φ_{jump} is reduced; meanwhile, the switch - ing transients are extended from t = 0 s to t = 4s in length under these conditions. An in-built trade-off exists:

$$P_{surge}\cdot\tau\approx constant \tag{6}$$

Reduction in surge amplitude but not elimination of root discontinuity still distributes this short-term energy over an extended period, thus extending converter fatigue and delayting grid connection. A widely adopted droop control scheme to regulate voltage in DC micro-grid systems. It updates the reactive power setpoint in response to a DC-bus-voltage variation error. During the mode switching process, the droop control loop is in conflict with the mode-transition-logic, frequently triggering nested-integrator-saturation and further increasing phase-shifting oscillation. Existing studies reporting improved off-grid performance have not

addressed bidirectional mode reversal. The reported 4.27% overshoot refers to load-step response within the same operational mode, not to cross-mode switching[6]. As required, therefore, a control method for Phase-Shift Discontinuities needs to be introduced.

3 Proposed Transient Phase-Shift Feedforward and Virtual Impedance Composite Control

3.1 Unified Control Architecture without Mode Switching

As a replacement for the two separated charge-and-discharge control loops, a unifying controller over the full bi-directional working range is presented here. The controller adjusts the phase shift φ to be a nonlinear function of the power shortage ΔP = P* – P, where P* represents the grid-supplied power command (positive indicates discharging while negative means charging)). Unified controller Structure is as follows:

A steady-state power regulator, implemented as a PI compensator, which generates the base phase-shift φ_{ss}.

A transient feedforward compensator that pre-shifts the phase-shift trajectory before mode reversal. An adaptive virtual impedance regulator that shape the output impedance during transients to suppress power oscillations.

The unified control law is expressed as:

$$\varphi^*(t)=\varphi_{ss}(t)+\varphi_{ff}(t)+\varphi_{vir}(t) \tag{7}$$

where φ_{ss} is the PI output, φ_{ff} is the feedforward compensation, and φ_{vir} is the virtual impedance correction.

3.2 Transient Phase-Shift Feedforward Compensator Design

We drive the phase-shift into a state of zero ahead of time to overcome the phase-shift zero-crossing dead zone problem in traditional switching. The central idea of this paper is that, under a voltage drop condition where φ<0 and a rise condition under which φ>0 pass through φ=0. Instead of having the controller cross a zero randomly after the remaining integrating state by accident, it sets up a scheduled zero-phase shift point deliberately.

The feedforward compensator observes the incoming mode reversal command and computes a transient phase-shift trajectory $\varphi_{ff}(t)$ that satisfies:

$$\varphi_{ff}(\mathrm{t})=\begin{cases}\varphi_c+k_{ff1}t, & t_0\le t<t_z\ (approachzero)\\ 0, & t=t_z\ (zerocrossing)\\ k_{ff2}(t-t_z), & t_z<t\le t_d\ (departzero)\end{cases} \tag{8}$$

where k_{ff1} and k_{ff2} are feedforward rates determined by the converter's current slew rate capability and the DC bus capacitance. The zero-crossing instant tz is explicitly enforced by the modulator, ensuring that the phase-shift ratio is precisely zero when the power command crosses zero.

Critically, the feedforward path operates in parallel with the feedback regulator. During the approach phase, the PI output φ_{ss} is gradually unloaded by the rising φ_{ff}, preventing integrator windup. At t_z, the total phase-shift $\varphi^* = \varphi_{ff}(t_z) + \varphi_{ss}(t_z) = 0$. The feedforward gain K_{FF} is defined as:

$$K_{FF}=\frac{|\varphi_c|}{T_{FF}} \tag{9}$$

where T_{FF} is the user-adjustable feedforward time constant. Selection of T_{FF} involves a trade-off: shorter T_{FF} yields faster transition but requires higher instantaneous current slew rate; longer T_{FF} reduces current stress but prolongs the zero-power interval. Analysis of the converter's small-signal model indicates that optimal T_{FF} approximates 3–5 switching cycles.

3.3 Adaptive Virtual Impedance Regulator

Although feedforward compensation removes the phase-shift discontinuities, the DAB output impedance and the DC bus network may still interact and cause post-switching power oscillations. Additionally, some works use adaptive virtual impedance regulators to solve issues at the moment of switching resulting from this approach.

The virtual impedance is implemented as a first-order high-pass filter applied to the DC bus voltage deviation:

$$\varphi_{vir}(s)=-Z_v(s)\cdot\Delta U_{dc}(s)=-\frac{k_v s}{s+\omega_v}\cdot\Delta U_{dc}(s) \tag{10}$$

where k_v is the virtual impedance gain and ω_v is the corner frequency. The high-pass characteristic ensures that virtual impedance remains inactive during steady state ($\Delta U_{dc} \approx 0$) but provides transient damping when bus voltage fluctuates.

The adaptation mechanism adjusts k_v based on the operating mode and SOC. During discharge-to-charge switching, k_v is temporarily increased to 2–3 times its nominal value, then exponentially decays to steady-state level within 0.5 s. This temporary boost improves damping precisely when the system is most susceptible to oscillation without affecting the accuracy of steady-state voltage regulation.

3.4 Composite Control Implementation

The unified controller receives the power command P* and measured power P, computes ΔP through the PI regulator to generate φ_{ss}. Simultaneously, a mode transition detector monitors the sign change of P*; upon detecting impending reversal, the feedforward trajectory generator is activated. The virtual impedance loop continuously processes U_{dc} measurement and injects φ_{vir}. The three components are summed and limited to $\varphi \in [-0.25, 0.25]$ before delivery to the digital pulse-width modulator.

The composite controller applies to existing hardware and incurs a minimal additional processing cost—most ramp feedforward and virtual impedance filtering are first-order in terms of computational cost. This makes the composite controller applicable to existing converter controllers with limited digital signal processing (DSP) capabilities.

4 Hardware-in-the-Loop Validation and Performance Evaluation

4.1 Experimental Setup

A hardware-in-the-loop validation Platform is established for testing the proposed control Technique under real-world Operation Conditions at The Plant Level. The Platform includes

the following parts: a real-time digital simulator that runs the 500-kw Dab converter and the DC micro-grid plant model with electromagnetic transient resolution at 2μs, as well as a TMS320f28379d Digital Signal Processor (DSP) based on the proposed control strategy, signal conditioner interface to simulate analog measurements; gate signal acquisition. Table 2 shows the parameters of the DAB Converter.

Table 2: DAB Converter Parameters

Parameter	Symbol	Value
Rated power	P_{rate}	500 kW
Battery voltage	U_{bat}	650–850 V
DC bus voltage	U_{dc}	750 V (nominal)
Switching frequency	f_s	10 kHz
Auxiliary inductance	L	55 μH
Transformer turns ratio	n	1:1
DC bus capacitance	C_{dc}	12 mF

Four kinds of operating conditions were designed for an overview of the transient performance: (1) Nominal power reversal under 50% state-of-charge; (2) Positive high state-of-charged (90%) charging-discharging switching; (3) Negative low state-of-charged (20%) discharging-recouping switch; (4) Power reversals between two levels, from +/-25% rated output. Evaluate the Design Approach based on a combination of three reference systems (classical PI-mode switching with rate limitation), Dropping Voltage Control without separate switching suppression), Unified Power Control mode used in previous adaptation for 500 kW.

4.2 Transient Response Characteristics

Under conventional PI control, the phase-shift exhibits a distinct discontinuity: the charging-mode PI controller is disabled, its integrator reset, and the discharging PI controller initialized with zero output. This process introduces a 12 ms interval during which φ remains at −0.12, followed by a step change to +0.08—a φ_{jump} of 0.20. Consequently, a 600-kW power surge (1.2 p.u.) is observed, accompanied by 48.7 V DC bus voltage drop and 1.21 s settling time.

While droop-only control marginally couples feedback for the bus voltage to reduce the surge to 510 kW, the phase-shift discontinuity occurs as a result of the mode-switching architecture that underlies it[7]. Unified control methods eliminate control loop switching, but do not employ zero-crossing scheduling, meaning control over phase-shift zero-crossing is dictated by the integrator, which leads to a 380-kW surge and a 0.61 s transient duration.

Composite control methods, such as the proposed one, make a fundamental change in the trajectory of transients. In this case, the compensator provides a feedforward function that, as soon as it detects a mode reversal, at t = 1.0 s, then modifies the function of φ to approach zero, and control the rate at which φ crosses zero to 0.015 ms -1, and so, at t = 1.018 s, φ will be zero. The phase-shift is then held at zero for 0.5 ms (5 cycles of switching), after which it is free to shift to a new steady-state value, thereby discontinuing the phase-shift. The trajectory of power is then able to pass through zero without obstruction and peak to only 153 kW (0.306 p.u.), a 74.6% improvement from the conventional control. The DC bus voltage deviation is minimized to 28.3 V (3.8%), and the transient duration τ is minimized to 0.28 s. Fig. 2 visually compares these key performance metrics under rated reversal condition. Table 3 provides a summary of the four test scenarios and a quantitative comparison.

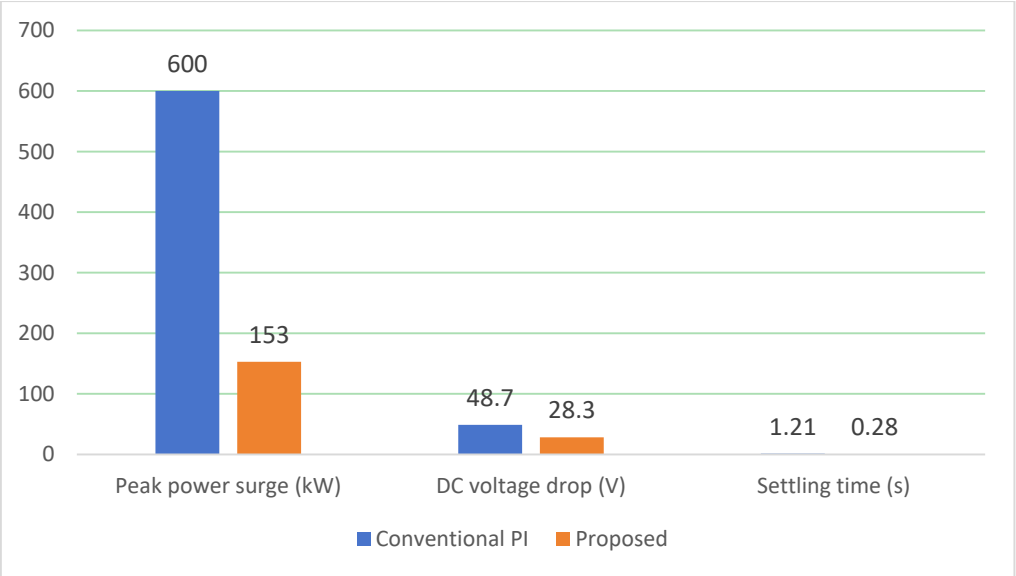

Figure 2: Performance comparison between conventional PI control and the proposed method

Table 3: Performance Comparison under Various Operating Conditions

Scenario	Method	P_{surge} (kW)	Udc Drop (V)	τ (s)
Rated Reversal (50% SOC)	Conventional PI	600	48.7	1.21
Rated Reversal (50% SOC)	Droop-only	510	41.2	0.95
Rated Reversal (50% SOC)	Unified Control	380	35.6	0.61
Rated Reversal (50% SOC)	Proposed Method	153	28.3	0.28
High SOC (90%)	Conventional PI	645	52.1	1.35
High SOC (90%)	Proposed Method	168	30.5	0.31
Low SOC (20%)	Conventional PI	572	46.8	1.18
Low SOC (20%)	Proposed Method	149	27.9	0.26
Partial Reversal	Conventional PI	315	29.4	0.82
Partial Reversal	Proposed Method	82	16.8	0.19

4.3 Virtual Impedance Contribution Analysis

To isolate the individual contributions of feedforward compensation and virtual impedance, an ablation study was conducted. Feedforward-only configuration (virtual impedance disabled) achieves P_{surge} = 195 kW and τ = 0.34 s; virtual-impedance-only configuration (feedforward disabled) yields P_{surge} = 290 kW and τ = 0.52 s. Both components contribute meaningfully, but feedforward plays the dominant role in eliminating the initial surge, while virtual impedance effectively damps the subsequent 10–30 Hz power oscillation otherwise present during the first 0.15 s after zero crossing[8].

The adaptive gain mechanism especially shows merit when high SOC conditions are present. For battery voltages of 850 V at 90% SOC, the same phase-shift results in an increase in power by 14% per (1). The virtual impedance gain is boosted by 2.3x automatically at the switching transient which results in proportionally more damping to address the increased sensitivity of the plant.

4.4 Robustness and Sensitivity Analysis

Studying the robustness of the method showed its effectiveness against parameter uncertainty

and the noise of measurements[9]. The feedforward rate k_{ff} was adjusted to ±40% of its nominal value. Within this range, the surge magnitude remains below 210 kW. This demonstrates that a precise understanding of system parameters is not necessary; the primary advantage comes from imposing a controlled zero crossing, not the specific slope of the trajectory.

DC bus capacitance was purposefully decreased by 30% in order to model converter aging or variability in manufacturing. With the proposed method, $P_{surge} < 190$ kW is achieved, while in conventional control, P_{surge} surges to 710 kW due to worsened voltage deviation. The virtual impedance directly reduces voltage dips which explains the partial offset for the lowered physical capacitance.

Performance is not materially degraded by measurement noise, which is emulated by adding ±1.5% random noise to the voltage and current feedback signals. The virtual impedance filter's high-pass characteristic will always reject DC and low-frequency noise, and the feedforward path is open-loop during the crucial 20 ms window and is protected from feedback corruption.

5 Discussion

5.1 Comparative Assessment and Theoretical Implications

The experimental findings support the main thesis: the power surge during charge–discharge switching is primarily an artifact of control rather than a physical given. The method introduced here, by rethinking bidirectional operation as a continuum rather than as two separate modes, removes the fundamental discontinuity that traditional methods try to lessen downstream[10].

A greater proportion, 74.6 per cent, of the rise was less than the 11-30 per cent range of fluctuation changes found in some investigations into flywheel UPS switching and household inverters transitions. The reason for this difference is mainly due to their different natures as switchings. Flywheel systems have a physical inertia during mode switching, and their current/voltage peaks are due to electrical angle offset; Angle compensation directly addresses this issue. On the other hand, DAB converts do not use any physical method for unidirectional switching; only structure is provided here. Therefore, in terms of mean, an absolute omission does not hold up better against this lack.

The suggested approach further differentiates itself from hybrid energy storage methods where fast transients are assigned to supercapacitors[11]. Those methods understand that batteries cannot deal with quick power reversals and modularize (supercapacitors and additional DC-DC converters) to circumvent the problem. This work shows that battery converters, when properly controlled, can perform rapid and seamless bidirectional transitions without further hardware. This is particularly important economically to plant-level storage, where supercapacitor-based hybrid systems are very costly and take up a lot of space.

5.2 Practical Implementation Considerations

A number of practical considerations are informative. The first is that feedforward compensators require information about upcoming mode reversals[12]. Regarding grid-following operation, power commands are sent in a fixed periodic manner (typically 20–100 ms). Therefore, a look ahead buffer of one dispatch interval is sufficient. As for grid-forming operation, droop frequency control of the grid passing a nominal value generates mode reversals; therefore, compensation is automatic, so prediction is redundant. The

compensator will respond to an instantaneous sign reversal of the internal power reference.

Second , there is the zero-power interval, the time duration during which φ is held at zero, and this causes a momentary halt in power delivery. The validation results indicate that a 0.5 ms interval (five switching cycles) is sufficient. For a 500-kW system, this translates to a total of 250 J of unused energy. In frequency regulation service, 2–4 s response time is standard, so the brief interruptions are of little significance. For applications that need a constant power supply, the duration of the zero interval can be shortened to a single switching cycle (0.1 ms) which will also decrease the zero interval duration (P_{surge} increases from 153 kW to 210 kW), providing a customizable trade-off.

Third, it was established that the method is compatible with existing communication and protection systems. The unified controller provides output of phase-shift commands that are identical in format and range to those of conventional controllers; supervisory controllers and protection logic receivers receive measurement signals that are unchanged. For retrofitting, the only requirement is the modification of firmware[13]. No hardware, communication protocols, or other systems need to be changed.

5.3 Limitations and Future Research Directions

Some existing limitations of this work indicate additional areas of research. The validation used only one DAB converter battery to DC bus. Typical large-scale storage systems have several parallel integrated converters with interleaved carriers and circulating current control. The questions regarding the multiple unified control interactions when the controllers are in different dispatches and mode reversals, such as when all the converters are set to the same dispatch, need to be studied. First, it has been observed that in such situations, the current slew rate is likely to be higher than the DC bus capacitor limit, thus requiring either staggered feedforward ramping or some form of communication to control the feedforward[14].

The approach relies on ideal voltage behavior on both the battery and the sides of the DC bus. Battery terminal voltage behavior during high current transients, especially the instantaneous impedance of lithium-ion cells, were simulated as a voltage source with series resistance. Such battery models, which are more advanced and include electrochemical components, polarization and diffusion, may show some more transient behavior which are not captured here. Extensions of the concepts to other bidirectional converter topologies are fairly simple conceptually, especially for three-phase dual-active-bridge and resonant CLLC converters, but those extensions will require topology specific phase shift to power relationship[15]. The unified control principle of maintaining continuous control across zero power, and maintaining a schedule for zero phase shift crossings, is topology agnostic, but the rate limit feedforward control needs to be re-derived for the small-signal model of a given topology.

6 Conclusion

A novel technique to suppress transients of power surges during switching modes of plant-level energy-storage converter has been introduced and verified experimentally. Analyses showed that the power spike was due to a combination of dual-mode operation instead of an intrinsic defect in DAB conversion components. The proposed composite control system tackles the aforementioned problem by integrating two methods: transients Feedforward compensation, which stabilizes the control of zero-phase-shift crossing; Adaptive virtual impedence control in conjunction with active increase in damping during the recovery period after the switching event.

Performing hardware-in-the-loop validation on a 500-kW DAB converter platform showed that the method reduces the peak power surge by 74.6%, compresses the duration of the switching transients by 76.9%, and keeps the DC bus voltage deviation within 3.8% for a wide range of SOC and power deficit conditions. Feedforward control is believed to be the main suppression mechanism from the studies, while virtual impedance is said to be the main mechanism for suppressing residual oscillation. The method is shown to demonstrate effectiveness in regards to uncertainties in parameters, measurement noise, and the aging effects of the converter.

This paper demonstrates that the battery storage converter has achieved smooth forward-and-reverse conversion with no extra components needed. This work disputes that surge of power occurs unavoidably at switching times in conversion devices and requires passive filter circuits or even hybrid SuperCapacitors to address the issue. Unified control model postulates a firmware-only approach that can be applied to both old and new storage systems for an agile and economical addition of grid-scale energy storage.

Author's Profile

Shiyu Zhang was born in Qinghai, China in 2004. She is currently studying at the School of Electrical and Electronic Engineering, Wenzhou University, with a focus on Electrical Engineering and Automation.

References

[1] Nalamati S C, Gupta R. Analytical investigation of interleaved input/output parallel DAB converter for grid scale battery storage[J].Journal of Energy Storage, 2024, 99(PB):113400-113400.

[2] Zhou K, Liu M, Zhang Y. A high-gain bidirectional DC/DC converter based on interleaved parallel DAB cascaded three-level Buck/Boost[J].Electric Power Systems Research, 2026, 254112701-112701.

[3] Chandrakar N, Sekhar C C, Mageshwari S, et al. Investigative study on peak current reduction with unified phase shifting technique in DAB converter[J].Electrical Engineering, 2025, 108(1):40-40.

[4] Zhang C, Zhu J, Ding X, et al. Optimal Hybrid Fault Tolerant Control With Voltage Balancing for IPOS DAB Converters[J].IET Power Electronics, 2025, 18(1):e70062-e70062.

[5] Ma H, Lei J, Qin G, et al. Efficiency Optimization Control Strategies for High-Voltage-Ratio Dual-Active-Bridge (DAB) Converters in Battery Energy Storage Systems[J].Energies, 2025, 18(10):2650-2650.

[6] Chen Z, Zheng Z, Tang X, et al. Model Predictive Controlled Dual Active Bridge Converter with Efficiency Optimization and Fast Dynamic Response[J].Journal of Electrical Engineering & Technology, 2024, 19(1):521-534.

[7] Nalamati S C, Gupta R . Frequency domain power flow characterization in lossy DAB converter for battery energy storage[J].Journal of Energy Storage, 2026, 150120426-

120426.

[8] Adriano N, Arthur A, Nelson S, et al. Adaptive Model Predictive Control for DAB Converter Switching Losses Reduction[J].Energies, 2022, 15(18):6628-6628.

[9] Pablo G, Nimrod V, Marco L, et al. Two-Stage Modulation Study for DAB Converter[J].Electronics, 2021, 10(21):2561-2561.

[10] Li T, Zhang Y, Sun J, et al.Simplified Universal Suppression Method for Transient DC Bias of DAB Converters With Multiple Phase-Shift Modulation[J].Power Electronics, IEEE Transactions on, 2025, 40(11-Part2):17246-17255.

[11] Hu J, Cui S, De Doncker R W .Natural Boundary Transition and Inherent Dynamic Control of a Hybrid-Mode-Modulated Dual-Active-Bridge Converter[J].IEEE Transactions on Power Electronics, 2022, 37.

[12] Yao N, Wang T, Duan B, et al. A simple but effective virtual inertia control for dual active bridge in DC microgrid to suppress voltage fluctuation[C]//2023 26th International Conference on Electrical Machines and Systems (ICEMS). IEEE, 2023: 328-332.

[13] Qin L, Wu T X, Xiao Y, et al. Input Stability Enhancement Strategies for Input-Series-Output-Parallel Dual-Active-Bridge Converter: Modeling, Reshaping, and Experiment[J]. IEEE Transactions on Transportation Electrification, 2025, 11(4):9512-9531.

[14] Li H, Zhang X, Jiang L, et al. Modified phase-shift scheme for optimal transient response of dual-active-bridge DC/DC converters considering the resistive impact[J]. IEEE Transactions on Power Electronics, 2021, 36(10): 12058-12072.

[15] Jung G G, Lee S J, Kim S H, et al. Design methodology of a voltage controller for a dual-active-bridge converter utilizing spread-spectrum modulation[J].Journal of Power Electronics, 2025, 25(3):1-12.